

NOTES AND CORRESPONDENCE

**Observations of the Relationship between 700-mb Temperatures and
Severe Weather Reports across the Contiguous United States**

MATTHEW J. BUNKERS, JOHN R. WETENKAMP, AND JEFFREY J. SCHILD
NOAA/National Weather Service, Rapid City, South Dakota

(Submitted to Weather and Forecasting 7 July 2009)

Under Review

Corresponding author address: Dr. Matthew J. Bunkers, National Weather Service, 300 East
Signal Drive, Rapid City, SD 57701-3800.

E-mail: matthew.bunkers@noaa.gov

ABSTRACT

The relationship between 700-mb temperatures and convective severe storm reports is examined using data from 1993–2006 for the contiguous United States. Motivation for this study derives from the often-used 12°C at 700 mb rule-of-thumb with respect to the extent and strength of the capping inversion. Whereas there is a semblance of merit for using this rule at times, it is of little value during the peak of the warm season and across high terrain. Calculation of convective inhibition, examination of the sounding, and assessment of lifting mechanisms are far more valuable than 700-mb temperatures when forecasting the potential for deep moist convection and severe storms.

1. Introduction

Forecasting whether a capping inversion will give way to deep moist convection remains a difficult problem for operational forecasters (Moller 2001, pp. 437–438; Wakimoto and Murphey 2009, pp. 912–913). Actually this is a two-pronged problem (McNulty 1995): Will thunderstorms initiate in a given area, or will mature thunderstorms be able to move into a given area?

Convective inhibition (CIN; Colby 1984) is a diagnostic variable that is used to assess the strength of the capping inversion. CIN is a measure of the energy associated with negatively buoyant air that rising parcels need to overcome in order to reach the level of free convection (LFC)—ultimately resulting in deep moist convection (DMC) once the LFC is reached. This negative energy typically is overcome through mesoscale and storm-scale processes, such as those brought about by boundaries, differential heating, and terrain influences (e.g., McNulty 1995; Moller 2001; Weckwerth and Parsons 2006; Kalthoff et al. 2009).

Moller (2001) stated that numerical model forecasts can produce CIN fields with considerable noise and uncertainty, which is in large part due to difficulties in properly measuring and forecasting low-level moisture (Weckwerth and Parsons 2006). Indeed, even model initial *analyses* of CIN can be plagued with inconsistencies (e.g., compare the four different model analyses in Fig. 1). And to complicate matters further, some software programs report notably different CIN values for the same sounding, such as when two LFCs are present (e.g., Fig. 2; one program might report the lower CIN–LFC pair, but another program might report the upper CIN–LFC pair).

Shortly after Colby (1984) introduced CIN, Graziano and Carlson (1987) evaluated the lid strength index [LSI, introduced by Carlson et al. (1980)] as a tool to quantify the capping inversion. They defined the LSI as the difference between the maximum saturation wet-bulb potential temperature at the warmest point in the inversion (θ_{sw1}) and the vertically averaged value of the wet-bulb potential temperature between 30 and 80 mb AGL ($\bar{\theta}_w$). The 90th percentile of the LSI from their study of DMC was 2.0°C, indicating a minimal probability of DMC when the LSI exceeds 2.0°C. Graziano and Carlson (1987) also found a paradoxical relationship whereby DMC is more likely when the LSI is small (near zero), yet the probability of severe local storms—conditional on DMC—increases with increasing LSI for a given value of buoyancy. The usage of CIN has prevailed over the LSI in the operational and research communities since the inception of these indices, perhaps because CIN is an integrated quantity instead of being dependent on a subset of sounding levels like the LSI.

Before the advent of more sophisticated computers and software routines in the 1990s—which enabled the routine calculation of CIN—forecasters considered 700-mb temperatures (hereafter T_{700}) as a simple guide for predicting the strength of the capping inversion. One reason for this is that the 700-mb level is slightly above the mean height of the typical capping inversion, especially across the High Plains. Since 700 mb also is a mandatory pressure level for radiosonde observations, this allows for a quick estimation of the capping inversion. In favor of this, an analysis of long-term records from seven sounding sites across the contiguous United States (CONUS, starred locations in Fig. 3) indicates that T_{700} is significantly correlated with CIN and the LSI (Table 1), but generally with weaker correlations for stations at lower elevations. Since CIN is defined as negative herein, a negative correlation between T_{700} and CIN indicates higher temperatures are associated with stronger capping.

Evidence for using T_{700} as a proxy for the capping inversion goes back to at least the 1950s. Means (1952, p. 173) suggested that “Thunderstorm activity seems to be damped under the warm ‘lid’ aloft at 700 mb....” Miller (1967, p. 6-4) later quantified this by stating: “During summer months the more significant storms appear to form north and northeast of the +10 to +14 [°C] isotherms at the 700-mb level.” Johns and Doswell (1992, p. 593) pointed out several limiting factors to DMC, one of which includes the following: “Deep convection is usually limited to those areas where the forecast 700-mb temperature (NGM) is colder than 12°C.” Johns and Doswell further cautioned that this empirical rule—which relates to the strength of the capping inversion, or CIN—does not apply at high surface elevations where the 700-mb level becomes part of the mixed layer.

In addition to these formal publications, there is a plethora of informal Internet-based materials pertaining to this subject¹. An Internet search, as well as our anecdotal operational evidence gained from reading many forecast discussions, suggests that the use of T_{700} to identify the capping inversion has not diminished in recent years (although it is our perception that CIN is used more widely than T_{700}). In particular, the 12°C isotherm at 700-mb has been used as a loose discriminator between environments with "storms" and those with "no storms"; seasonally varying temperature thresholds also are cited in these informal references (e.g., Davies 2009). In spite of this usage, one can find soundings associated with DMC that display a rather high T_{700} , but with minimal CIN (e.g., Fig. 4a, $T_{700} > 17^{\circ}\text{C}$). Conversely, T_{700} may be well below the

¹ An Internet search for “700mb temps capping” will bring up a myriad of examples with 700-mb temperatures used in discussions that are related to thunderstorm development/occurrence.

perceived “threshold” value, yet the CIN is exceptional and thus DMC is precluded (e.g., Fig. 4b, $T_{700} < 6^{\circ}\text{C}$). These two examples provide motivation for eschewing 12°C at 700 mb as a sole capping discriminator.

The purpose of this note is twofold: (1) remind forecasters that many storms do occur when T_{700} is well above 12°C ; and (2) provide a climatology so forecasters have a reference in case they choose to use T_{700} as an ancillary guide for capping and forecasting DMC. This will be done in a circuitous fashion by examining severe storm reports, which are predicated on convective initiation; the caveats of this methodology are discussed in section 4. Instead of using T_{700} , we advocate looking at other fields such as CIN, 0–2-km lapse rates, the LSI, or even the 700-mb lifted index to evaluate the strength of the capping inversion²—both with soundings and plan-view displays. Nevertheless, it may be that T_{700} provides some marginally useful local upper bound on DMC. It is further hypothesized that the appropriate T_{700} value depends on what type of severe weather is considered, such that the T_{700} threshold might be higher for severe wind than for severe hail. For these reasons, in addition to the perceived misuse of T_{700} , we believe it is important to quantify this rule-of-thumb that apparently has been, and continues to be, at least moderately used.

² Visible satellite images can provide useful qualitative information on the strength of capping inversions, in particular for short-term (0–3 h) forecasts. For example, interactions of horizontal convective rolls with other boundaries often portend DMC (Weckwerth and Parsons 2006), whereas laminar billow/wave clouds are a good indicator of a stable boundary layer (Bikos et al. 2002)—and thus a limited potential for DMC.

2. Data and methods

All convective severe storm reports for March–October from 1993–2006 for the CONUS (Fig. 3) were obtained from the National Oceanic and Atmospheric Administration (NOAA) *Storm Data* resource using the SVR PLOT software (Hart 1993). This search yielded 297,086 reports (Table 2), most of which are confined to the eastern two-thirds of the CONUS [similar to Brooks et al. (2003, their Fig. 4) and Doswell et al. (2005, their Figs. 5 and 6)]. Some of the severe wind reports from 1993–2002 were listed as “damage” instead of possessing a numerical value; herein these were assigned a nominally severe value of 25.7 m s^{-1} (50 kt), which may be an overestimate in some cases where shallow-rooted trees in moist soil were toppled by sub-severe winds. The severe reports then were subdivided into “significant” categories according to the criteria of Hales (1988): tornado rating $\geq \text{F2}$; hail with diameter $\geq 5.1 \text{ cm}$ (2 in.); and wind gusts $\geq 33.4 \text{ m s}^{-1}$ (65 kt). This resulted in 1400 significant tornado reports, 7137 significant hail reports, and 9411 significant wind reports (Table 2), which collectively comprise 17,948 (or 6%) of all severe reports herein.

Next, each individual severe report was matched in time and space with (i) the value of T_{700} and (ii) the 0–180-mb AGL most-unstable CIN (MUCIN³) from the 3-h, 32-km gridded North

³ To find the most-unstable “parcel,” the lowest 180 mb of the NARR atmosphere is divided into six 30-mb deep layers, and then the average thermodynamics are computed for each layer. The layer with the largest equivalent potential temperature (θ_e) is lifted using that layer’s values to compute the MUCIN (G. Manikin, 2009, personal communication), which has attributes of mixed-layer CIN. This is not be confused with the MUCIN methodology given in Table 1.

American Regional Reanalysis (NARR; Mesinger et al. 2006). Although the primary focus of the present study is on T_{700} and severe storm reports, MUCIN also is considered since it is a more robust measure of the capping inversion than is T_{700} (i.e., it is an integrated quantity associated with the energy needed to overcome the cap; see section 1).

Using geographic information system (GIS) software, the spatial distributions of the maximum and average T_{700} for a variety of report combinations (e.g., all hail, significant tornadoes, 1800–0600 UTC, etc.) were derived across the CONUS for a grid with spacing of roughly 80 km (e.g., Brooks et al. 2003; Doswell et al. 2005; Ashley et al. 2008). The same process was repeated for the MUCIN data, except that the minima were computed instead of the maxima (because CIN is defined as negative herein). At least five reports were required per grid box, with the exception of significant tornadoes where only one report was required per grid box. This latter constraint was a tradeoff between sample size (Table 2, cf. the “Sig” values in the last row) and geographical coverage; the entire significant tornado grid is only 25% of the area of the entire significant hail grid if five reports per grid box are required for both. This methodology dictates that caution must be used when interpreting the results for the significant tornado dataset. Because of this, monthly distributions were not constructed for the significant categories.

Additional 9-point smoothing of the T_{700} and MUCIN data was applied in order to bring out more clearly the spatial pattern in the results. This process mitigated the effects of relatively data sparse areas by allowing them to be influenced by neighboring grids containing more robust data. On the other hand, local extrema sometimes were reduced modestly when surrounded by valid boxes with relatively few reports—such that the extrema in neighboring boxes likely were not captured. The net effect is that when viewing the monthly smoothed data, local maxima of

T_{700} tend to be reduced by 0.75–1.75°C over the raw data; this is equivalent to the standard deviation of the differences between the smoothed and unsmoothed monthly data. For graphs including all months (March–October) the reduction is 1.25–2.75°C.

Caveats associated with the convective severe storm report database are discussed in Brooks et al. (2003), Doswell et al. (2005), and Verbout et al. (2006), among many other formal and informal papers. These three studies documented an increase in the number of all severe reports since the mid 1950s—ranging from a factor of two to an order of magnitude. Conversely, the annual number of significant severe reports has experienced minimal change during the same time period. Biases in the storm report database have arisen largely from population density variations, differences and trends in local verification efforts/methods, the burgeoning number of storm enthusiasts, and technological advances that make storm reporting easier. Even though the severe storm report database is fraught with uncertainty, the errors most strongly influence time series analyses, which are not being conducted in the present study. Nevertheless, the aforementioned smoothing of T_{700} and MUCIN is intended to account, in part, for spatial reporting biases that undoubtedly affect the results herein.

Another potential concern in the present study is spurious grid-scale precipitation in the NARR dataset (West et al. 2007). This is most pronounced from 2003 onward when the NARR analysis system changed with respect to the input precipitation and ice cover datasets. Reprocessed data from 2003–2006 were used herein, but this does not preclude the occurrence of spurious grid-scale precipitation (West et al. 2007). Fortunately, T_{700} is relatively unaffected compared to MUCIN since the former is independent of moisture. Furthermore, only 20% of all reports in this study occurred during 2003–2006, and of these only ~13.5% potentially would be affected by spurious grid-scale precipitation (i.e., <3% of the entire dataset; see West et al.

2007). All things considered, the spatially and temporally consistent NARR dataset was preferred over the relatively coarse network of radiosondes [which have their inherent limitations, e.g., Schwartz and Doswell (1991)] in order to increase the sample size.

3. Results and discussion

a. T_{700} and all severe storm reports

The results for all severe storm reports show a clear propensity for greater T_{700} as one goes from lower to higher surface elevations (cf. Figs. 3 and 5). Indeed, the correlation coefficient between surface elevation (Fig. 3) and the smoothed maximum T_{700} for all severe storm reports (Fig. 5) is 0.57, which is significantly ($\alpha < 0.001$) different from zero based on a Student's t test (Wilks 1995). This is not surprising because the 700-mb level becomes part of the mixed layer at relatively high and arid elevations where sensible heat fluxes can strongly influence T_{700} (Carlson 1998, pp. 449–457). In such environments the capping inversion might not even exist, and if it does, it typically exists above 700 mb. The largest area of the highest T_{700} exists over Colorado, just east of the Front Range, which is an area where the elevated mixed layer (EML) frequently overruns low-level moist air from the Gulf of Mexico.

Contrary to the general rule that 12°C at 700 mb is a limiting factor for DMC, 64% of the area with data in Fig. 5 has maximum $T_{700} > 12^{\circ}\text{C}$ —covering much of the western and central CONUS. The only place where this 12°C guideline consistently applies as an upper bound for DMC is over (i) the far western CONUS and (ii) the eastern one-quarter of the CONUS. Moreover, 10% of the CONUS from the High Plains to the southern Rockies has maximum T_{700}

>17°C (Fig. 5; 15% for the unsmoothed data). Maximum values of T_{700} from the raw data are 20.4°C for tornadoes, 20.6°C for hail, and 21.1°C for wind. Even the smoothed *average* T_{700} for the entire dataset has 2% (14%) of the CONUS with temperatures >12°C (>10°C); this area is confined mostly to the central and southern Rockies (refer to the Internet address in the Fig. 5 caption for this image).

Although severe thunderstorm events can occur across a significant portion of the CONUS with $T_{700} > 12^\circ\text{C}$, one might argue that this doesn't happen very often. This is especially true during the cooler months when the 95th percentile of T_{700} with severe storms is 5.4°C in March, 7.2°C in April, and 9.0°C in October; the maximum T_{700} for any severe report in March is 12.2°C, and in October it is 12.4°C. However, during the warmest months of July and August the 95th percentiles reach 13.9 and 13.0°C, respectively (Fig. 6). What is more, T_{700} is >12°C (>14°C) for 6.1% (1.8%) of all reports in the CONUS for the dataset herein; in July this increases to 14.1% (4.8%).

The High Plains is an area of the CONUS that receives a significant fraction of the total severe storm reports (e.g., Brooks et al. 2003; Doswell et al. 2005), and considering Fig. 5 this area deserves further investigation. Looking at a subset of the High Plains (i.e., the rectangular area in Fig. 3), the frequency of severe reports with $T_{700} > 12^\circ\text{C}$ is a nontrivial 25.7% (Fig. 7). When the June–August period is considered collectively, this frequency rises to 37.4%. Although many of these storms likely are high-based, that does not necessarily mean they are elevated whereby their inflow is above a surface-based stable layer (Corfidi et al. 2008). Clearly, if forecasters rely solely on the $T_{700} > 12^\circ\text{C}$ rule-of-thumb for capping across the High Plains, they will be led astray on many occasions.

The results from April–September show a seasonal cycle to the maximum T_{700} associated with severe storm reports, which is most conspicuous across the central CONUS (Fig. 8). As expected this mirrors the climatology of T_{700} , with the highest values occurring during the warmest time of the year. This annual cycle of maximum T_{700} —along with that shown in Fig. 6—is in accord with the general seasonal guidelines for T_{700} and capping proposed by Davies (2009). As in Fig. 5, the highest values of T_{700} consistently are located over the central Rockies and High Plains; during July an area of smoothed maximum $T_{700} > 15^{\circ}\text{C}$ extends from Canada to Mexico (Fig. 8d). The spread of smoothed maximum T_{700} among various months also is largest over the High Plains (e.g., $\sim 11.5^{\circ}\text{C}$ difference between April and July over eastern Colorado) compared to areas such as the southeastern CONUS (e.g., $\sim 3^{\circ}\text{C}$ difference between April and July over Georgia). Again, this is a reflection of the EML that climatologically originates over the central and southern Rocky Mountains and passes over the High Plains, yet infrequently reaches the eastern CONUS (Carlson 1998, pp 462–463).

The diurnal cycle of T_{700} is dominated by severe storm reports from 1800–0600 UTC; 84.2% fall during this time frame, which has a smoothed maximum T_{700} pattern nearly identical to Fig. 5. However, a notable diurnal difference still emerges whereby the maximum T_{700} is lower during 0600–1800 UTC than during 1800–0600 UTC (refer to the Internet address in the Fig. 5 caption for these images). This is especially true across the High Plains where differences in maximum T_{700} between these two time periods range from 2–8°C. Comparisons cannot be made across most of the Rocky Mountains because of the dearth of reports there between 0600–1800 UTC. Across the eastern half of the CONUS the differences generally are 1–2°C (i.e., higher during 1800–0600 UTC). And for average T_{700} the diurnal differences are ± 1 –2°C for nearly all of the central and eastern CONUS.

In summary, results presented in this section elucidate that (i) the relationship between T_{700} and the occurrence of severe convective storms is strongly tied to topography and (ii) values of $T_{700} > 12^{\circ}\text{C}$ are not uncommon in severe thunderstorm environments, especially across the High Plains and Rocky Mountains during the warm season.

b. T_{700} versus severe storm report type

Variations in maximum T_{700} are evident among the three different severe storm report types, as well as between significant and non-significant categories (e.g., Fig. 9). First, it is evident that the smoothed maximum T_{700} generally increases from tornadoes to hail, and from hail to wind. The differences are mainly from $1\text{--}3^{\circ}\text{C}$ across the central CONUS for tornadoes and hail (cf. Figs. 9a and 9c), but are smaller for hail and wind with $0\text{--}2^{\circ}\text{C}$ increases in the smoothed maximum T_{700} for wind over the central and eastern CONUS (cf. Figs. 9c and 9e). The exception is Florida where this trend is reversed with a $1\text{--}2^{\circ}\text{C}$ decrease from tornadoes to wind. Second, similar changes/increases in the smoothed maximum T_{700} are observed among the significant tornado, hail, and wind categories (Figs. 9b, 9d, and 9f). However, in this case the increase of maximum T_{700} is larger from significant tornadoes to significant hail (i.e., $1\text{--}6^{\circ}\text{C}$) than it was for all tornadoes to all hail, with the largest increases ($3\text{--}6^{\circ}\text{C}$) confined primarily to the central CONUS.

The distribution of the raw severe storm reports versus T_{700} —grouped into classes according to damage/severity (Fig. 10)—supports the trends noted above. Specifically, the maximum T_{700} values increase for each category from tornado to hail to wind. Furthermore, the decile plots show a contraction of the distributions from the less damaging/weaker events (left side of Fig.

10) to the most damaging/strongest events (right side of Fig. 10). Not only does the maximum T_{700} decrease with increasing damage/severity of the reports (as was the case in Fig. 9), but the minimum T_{700} increases concurrently, primarily for tornado and hail reports.

Another interesting aspect of Fig. 10 is the clustering of the middle 80% of the distributions: (i) 1.5–11°C for tornadoes; (ii) 1–12°C for hail; and (iii) 3–13°C for wind. From this perspective it becomes apparent why the 12°C threshold for DMC gained support; 90% of the distributions are below 12–13°C, concordant with Johns and Doswell's (1992) statement in section 1. Furthermore, no F4–F5 (F2–F3) tornadoes were recorded with $T_{700} > 12^\circ\text{C}$ ($> 14^\circ\text{C}$), and only 5% of all tornadoes from 1993–2006 are associated with $T_{700} > 12^\circ\text{C}$ (6.8% and 5.6% for all hail and wind, respectively). This amounts to an average of just 54 out of 1092 tornadoes per year with $T_{700} > 12^\circ\text{C}$. By way of comparison, the frequency of $T_{700} > 12^\circ\text{C}$ with significant tornadoes, significant hail, and significant wind is 2.6%, 9.0%, and 11.3%, respectively. Conditional upon a reported tornado, the empirical probability of a significant tornado is ~0.1% when $T_{700} > 12^\circ\text{C}$. Keep in mind, however, that Fig. 10 is based on the entire dataset; the distributions are shifted higher for the central CONUS and Rocky Mountains, as well as for the warmer months of the year (e.g., refer to Figs. 6 and 7).

There is at least some physical explanation for the above observations. First, with respect to wind production, steep low-level lapse rates favor downward transport of vertical momentum (e.g., Wakimoto 1985). Therefore, T_{700} can be rather high, but if the capping inversion has been eroded and DMC is produced (e.g., Fig. 4a), severe wind-producing storms, such as dry microbursts, can result. Even derechos can occur when the average T_{700} is relatively high (e.g., Johns and Hirt 1987), with the climatological maximum of derechos along the northeastern edge of the warmest T_{700} . Second, the development of severe hail requires significant buoyancy for

strong updrafts, and a melting level that is not exceedingly high above the ground (e.g., Knight and Knight 2001). As buoyancy diminishes and the melting level increases above a given threshold (which is typical of environments with high T_{700}), the proclivity for severe hail wanes. This suggests that T_{700} would not be as high, on average, for severe-hail environments compared to severe-wind environments (or for significant severe hail versus all severe hail). Last, recent research suggests that low lifted-condensation-level (LCL) heights are more favorable for tornadogenesis than high LCL heights, especially for significant tornadoes (e.g., Markowski et al. 2002; Thompson et al. 2003). In order to attain low LCL heights and also reduce the strength of the capping inversion so DMC can be achieved—in the presence of high T_{700} —an exceptional amount of low-level moisture is needed. This is not a routine occurrence in the atmosphere; hence tornadic storms, relative to severe hail- and wind-producing storms, tend to favor environments with lower T_{700} where these low-LCL and low-CIN environments are more attainable⁴.

In summary, as T_{700} increases, DMC is less likely to be sustained in environments with low LCL heights (which tend to favor tornadogenesis). And as T_{700} increases further, production of severe hail is less efficient because of melting and possibly less buoyancy.

⁴ Although it is beyond the scope of this study, it is possible that the difference between Figs. 9a and 9b represents two different tornadogenesis processes in the High Plains: nonsupercell tornadoes in the warmer T_{700} environments (Fig. 9a) versus supercell tornadoes in the cooler T_{700} environments (Fig. 9b). Nonsupercell tornadoes can occur with relatively high cloud bases and LCL heights—a condition presumably more common when T_{700} is high.

c. MUCIN and severe storm reports

Only a small subset of the MUCIN results is presented here because these results are not the focus of the present study. However, considerable additional information is available at the Internet address provided in the Fig. 5 caption. The intent here is only to point out the most apparent contrasts between using T_{700} and CIN when determining characteristics of the capping inversion.

Consistent among all of the MUCIN versus severe-storm-report results is a maximum of absolute values across the central CONUS, whether this is for minimum MUCIN or for average MUCIN (e.g., Fig. 11). In particular, the “High Plains” region (outlined in Fig. 3) has notably larger negative values of MUCIN when compared to the rest of the CONUS (Fig. 12, dotted line); Graziano and Carlson (1987) found a similar result. It is likely that this climatological extreme in MUCIN (and capping) is a result of the advection of the EML over the central CONUS—producing the familiar “loaded gun” type I sounding (Miller 1967).

Like for T_{700} there is a significant, albeit somewhat weaker, correlation between elevation and the smoothed minimum MUCIN ($r = 0.44$; also cf. Figs. 3 and 11), meaning that as elevation increases, the strength of the capping generally decreases. After closer inspection it appears this correlation coefficient is misleading, however, as average MUCIN becomes stronger/more negative from the eastern CONUS to the central CONUS (Fig. 11)—suggesting the correlation is negative in this area. In fact, the correlation coefficient between elevation and minimum MUCIN is -0.25 when conditional on elevation < 750 m; this region comprises mainly the eastern half of the CONUS and a narrow zone along the west coast (refer to Fig. 3). On the other hand,

the correlation coefficient is 0.55 when conditional on elevation >750 m. In agreement with these results, the scatter plot of these two variables is conspicuously nonlinear (not shown). This pattern differs from what was shown for smoothed maximum T_{700} (Fig. 5) where the largest values were shifted unequivocally toward the highest terrain, implying that the strength of the capping inversion was strongest there.

Another contrast between the results of T_{700} and MUCIN is that the seasonality of MUCIN is much less pronounced (e.g., Fig. 12); the patterns of MUCIN show minimal contrast among the monthly curves from April to September. Likewise, Graziano and Carlson (1987) found little significant seasonal variation for critical values of the LSI, except for slightly higher values during the early spring. This result should be expected for a physically based measure of the capping inversion such as CIN and LSI. Note also that the cumulative frequency distribution functions (CDFs) are of exponential type in Fig. 12, indicating that most of the severe events occurred with relatively small capping. Indeed, 70% of the CONUS events occurred with MUCIN between -24.0 and 0 J kg^{-1} (this range is between -45 and 0 J kg^{-1} for the “High Plains”). Compare this to Fig. 6 where the CDFs rise sharply after they reach a given threshold, and then tail off gradually for extreme values of T_{700} .

The last distinction to be drawn between T_{700} and MUCIN is the diurnal variation. Although values of T_{700} decrease during 0600–1800 UTC (suggesting weaker capping), MUCIN actually becomes stronger overnight, especially across the central CONUS. Similarly, Graziano and Carlson (1987) noted LSIs were slightly higher at 1200 UTC relative to other times. It is believed this is a consequence of nocturnal cooling in the boundary layer beneath air with relatively high values of T_{700} associated with the EML, which results in climatologically stronger CIN at night. The fact that severe storms—perhaps mostly elevated—can still occur in the

presence of this significant CIN overnight may be related to strengthening of the nocturnal low-level jet and its ability to act as a strong lifting mechanism (e.g., Bonner 1966).

In summary, it is apparent that CIN is (i) climatologically strongest in the central CONUS, (ii) a more reliable indicator of the capping inversion than T_{700} , and (iii) not strongly dependent upon elevation or time of year with respect to convective severe storm reports.

4. Conclusions and summary

The main emphasis of the present study was to compare T_{700} with convective severe storm reports across the CONUS. Admittedly this is a straightforward study, but one that needs to be done nonetheless considering the continued application of T_{700} to capping and DMC. Based on the above results, the following conclusions are made:

- Many areas of the CONUS, especially the Rockies and High Plains in summer, experience DMC and severe convective storms with T_{700} well above 12°C .
- The greater the surface elevation, the less relevant and reliable the $T_{700} > 12^{\circ}\text{C}$ rule-of-thumb becomes for assessing the extent and strength of the capping inversion.
- Forecasters should not use T_{700} as a primary guide for forecasting (i) the initiation of DMC or (ii) the occurrence of severe storm events.
- CIN is a much more reliable indicator of the capping inversion than is T_{700} —caveats associated with accurately representing thermodynamics in the boundary layer notwithstanding.

It is important to discuss what this study does not represent. First, it does not address convective initiation per se as it relates to T_{700} because we chose to look at severe storm reports instead of lightning, radar, or satellite data to see where storms first developed. In other words, using T_{700} in the context of the present study is conditional upon convective initiation *plus* the reporting of severe weather. This means that if convection developed but did not produce severe weather, then that event would not be included in our database. Furthermore, the report locations may not indicate where convection developed, but rather where it became severe (i.e., the advection scenario stated at the beginning of section 1). Second, no attempt was made to stratify T_{700} by storm type (e.g., supercell versus nonsupercell, elevated versus surface-based, etc.). This is beyond the scope of this note, although it may provide useful information, such as possibly illustrating that nonsupercells produce most of the tornadoes when $T_{700} > 15^{\circ}\text{C}$ —tornadoes that almost exclusively are F0–F1. Last, T_{700} was not used explicitly to discriminate between tornadic and nontornadic storms. Prior work (e.g., Davies 2004) has shown that the frequency of F1–F4 tornadoes decreases with increasing absolute values of CIN, which is suggestive of larger values of T_{700} (refer to Table 1). Consistent with this, minimal evidence exists herein to proffer that F4–F5 tornadoes do not occur when $T_{700} > 12^{\circ}\text{C}$. Nevertheless, relying solely on T_{700} to predict tornado occurrence or nonoccurrence is unwarranted.

There are several reasons why T_{700} can fail at defining the capping inversion. First, the thermodynamic profile below the capping inversion in the boundary layer is critical to assessing whether DMC can develop. Moisture variations below the capping inversion in particular can result in varying thresholds for T_{700} (assuming the LCL is below 700 mb). For example, if the boundary layer is relatively dry with low θ_e , it will be difficult for a parcel to possess small CIN, no matter how low the T_{700} might be (e.g., Fig. 4b). However, T_{700} can be exceptionally high,

but if the atmosphere is well-mixed and the boundary layer θ_e is sufficient to produce positive buoyancy (e.g., Fig. 4a), DMC can develop. Second, the strength of the mesoscale and smaller-scale forcing determines how high a parcel can be lifted. With weak (strong) forcing it will be relatively difficult (easy) for a parcel to reach the LFC even if the T_{700} is low (high). Third, DMC may initiate above the 700-mb level in the form of elevated thunderstorms. In this instance it makes no sense to view T_{700} to determine the amount of capping. Clearly, manifold components—not necessarily independent of one another—need to be considered when assessing the capping inversion.

Considerable evidence has been presented herein to discourage the exclusive use of T_{700} to assess the extent and strength of the capping inversion. Nevertheless, there may be times when this simple variable might be beneficial as an adjunct when assessing the capping inversion, as well as a tool to monitor the spatial extent of the EML. For example, at long forecast projections (e.g., >24–36 h) when the boundary layer profile is not well forecast, it may behoove a forecaster to look at T_{700} to get an estimate of the capping inversion based on the time of year and location in the CONUS, capitalizing on the climatology that has been presented here. Another situation when T_{700} potentially may be useful is by comparing values of T_{700} to severe storm reports from the previous day, and then using that as a general guideline for the current day's forecast for the same geographic area—assuming the boundary layer hasn't changed appreciably. In summary, forecasting capping and DMC may be assisted by consulting T_{700} from the perspective of climatology and tracking the EML, respectively, but the physically relevant variables (e.g., CIN) and methods (e.g., sounding analysis) should take precedence over T_{700} .

Acknowledgments. We are indebted to the following individuals for their help with this research project: (i) Steve Weiss, Stephen Corfidi, and Dan Lindsey for providing background information and references; (ii) Phil Schumacher for his support with gempak and NARR data, as well as for his early discussions on this project; (iii) Al Pietrycha for providing the data for Fig. 1; (iv) Geoff Manikin for providing information on the NARR MUCIN calculations; (v) Chuck Doswell, Roger Edwards, Jonathan Garner, Patrick Kerrin, Jeff Passner, Harald Richter, Glen Romine, Jeff Snyder, Greg Stumpf, and Rich Thompson for correspondence on the usage of 700-mb temperatures for capping; and (vi) Kyle Carstens, Eric Helgeson, Jeff Johnson, Jeff Manion, Paul Smith, and Jon Zeitler for providing a review of this manuscript. We also would like to thank Dave Carpenter (Meteorologist-in-Charge, WFO Rapid City, South Dakota) for supporting this work.

REFERENCES

- Ashley, W. S., A. J. Krmenc, and R. Schwantes, 2008: Vulnerability due to nocturnal tornadoes. *Wea. Forecasting*, **23**, 795–807.
- Bikos, D., J. Weaver, and B. Motta, 2002: A satellite perspective of the 3 May 1999 Great Plains tornado outbreak within Oklahoma. *Wea. Forecasting*, **17**, 635–646.
- Bonner, W. D., 1966: Case study of thunderstorm activity in relation to the low-level jet. *Mon. Wea. Rev.*, **94**, 167–178.
- Brooks, H. E., C. A. Doswell III, M. P. Kay, 2003: Climatological estimates of local daily tornado probability for the United States. *Wea. Forecasting*, **18**, 626–640.
- Carlson, T. N., 1998: *Mid-Latitude Weather Systems*. American Meteorological Society, 507 pp.
- _____, R. A. Anthes, M. Schwartz, S. G. Benjamin, and D. G. Baldwin, 1980: Analysis and prediction of severe storms environment. *Bull. Amer. Meteor. Soc.*, **61**, 1018–1032.
- Colby, F. P., Jr., 1984: Convective inhibition as a predictor of convection during AVE-SESAME II. *Mon. Wea. Rev.*, **112**, 2239–2252.
- Colby, F. P., Jr., 1984: Convective inhibition as a predictor of convection during AVE-SESAME II. *Mon. Wea. Rev.*, **112**, 2239–2252.
- Corfidi, S. F., S. J. Corfidi, and D. M. Schultz, 2008: Elevated convection and castellanus: Ambiguities, significance, and questions. *Wea. Forecasting*, **23**, 1280–1303.
- Davies, J. M., 2004: Estimations of CIN and LFC associated with tornadic and nontornadic supercells. *Wea. Forecasting*, **19**, 714–726.

_____, cited 2009: Using 700mb temperatures as an estimation of the “cap” and to limit tornado potential. [Available online at:

<http://members.cox.net/jondavies1/700mbTcap/700mbTcap.htm>.]

Doswell, C. A., III, and E. N. Rasmussen, 1994: The effect of neglecting the virtual temperature correction on CAPE calculations. *Wea. Forecasting*, **9**, 625–629.

_____, H. E. Brooks, and M. P. Kay, 2005: Climatological estimates of daily local nontornadic severe thunderstorm probability for the United States. *Wea. Forecasting*, **20**, 577–595.

Graziano, R. H., and T. N. Carlson, 1987: A statistical evaluation of lid strength on deep convection. *Wea. Forecasting*, **2**, 127–139.

Hales, J. E. Jr., 1988: Improving the watch/warning program through use of significant event data. Preprints, *15th Conf. on Severe Local Storms*, Baltimore, MD, Amer. Meteor. Soc., 165–168.

Hart, J. A., 1993: SVR PLOT: A new method of accessing and manipulating the NSSFC severe weather database. Preprints, *17th Conf. Severe Local Storms*, St. Louis, MO, Amer. Meteor. Soc., 40–41. [Software available online at: <http://www.spc.noaa.gov/software/svrplot2/>.]

Johns, R. H., and W. D. Hirt, 1987: Derechos: Widespread convectively induced windstorms. *Wea. Forecasting*, **2**, 32–49.

_____, and C. A. Doswell III, 1992: Severe local storms forecasting. *Wea. Forecasting*, **7**, 588–612.

Kalthoff, N., B. Adler, C. Barthlott, U. Corsmeier, S. Mobbs, S. Crewell, K. Träumner, C. Kottmeier, A. Wieser, V. Smith, and P. Di Girolamo, 2009: The impact of convergence zones on the initiation of deep convection: A case study from COPS. *Atmos. Res.*, **93**, 680–694.

- Knight, C. A., and N. C. Knight, 2001: Hailstorms. *Severe Convective Storms. Meteor. Monogr.*, No. 50, Amer. Meteor. Soc., 223–254.
- Markowski, P. M., J. M. Straka, and E. N. Rasmussen, 2002: Direct surface thermodynamic observations within the rear-flank downdrafts of nontornadic and tornadic supercells. *Mon. Wea. Rev.*, **130**, 1692–1721.
- McNulty, R. P., 1995: Severe and convective weather: A Central Region forecasting challenge. *Wea. Forecasting*, **10**, 187–202.
- Means, L. L., 1952: On thunderstorm forecasting in the central United States. *Mon. Wea. Rev.*, **80**, 165–189.
- Mesinger, F., and Coauthors, 2006: North American Regional Reanalysis. *Bull. Amer. Meteor. Soc.*, **87**, 343–360.
- Miller, R. C., 1967: Notes on analysis and severe-storm forecasting procedures of the Military Weather Warning Center. Air Weather Service Tech. Rep. 200, Air Weather Service, Scott Air Force Base, IL, 140 pp.
- Moller, A. R., 2001: Severe local storms forecasting. *Severe Convective Storms, Meteor. Monogr.*, No. 50, Amer. Meteor. Soc., 433–480.
- Schwartz, B. E., and C. A. Doswell III, 1991: North American radiosonde observations: Problems, concerns, and a call to action. *Bull. Amer. Meteor. Soc.*, **72**, 1885–1896.
- Thompson, R. L., R. Edwards, J. A. Hart, K. L. Elmore, and P. Markowski, 2003: Close proximity soundings within supercell environments obtained from the Rapid Update Cycle. *Wea. Forecasting*, **18**, 1243–1261.
- Verbout, S. M., H. E. Brooks, L. M. Leslie, and D. M. Schultz, 2006: Evolution of the U.S. tornado database: 1954–2003. *Wea. Forecasting*, **21**, 86–93.

- Wakimoto, R. M., 1985: Forecasting dry microburst activity over the high plains. *Mon. Wea. Rev.*, **113**, 1131–1143.
- _____, and H. V. Murphey, 2009: Analysis of a dryline during IHOP: Implications for convective initiation. *Mon. Wea. Rev.*, **137**, 912–936.
- Weckwerth, T. M., and D. B. Parsons, 2006: A review of convection initiation and motivation for IHOP_2002. *Mon. Wea. Rev.*, **134**, 5–22.
- West, G. L., W. J. Steenburgh, and W. Y. Y. Cheng, 2007: Spurious grid-scale precipitation in the North American Regional Reanalysis. *Mon. Wea. Rev.*, **135**, 2168–2184.
- Wilks, D. S., 1995: *Statistical Methods in the Atmospheric Sciences*. Academic Press, 467 pp.

FIGURE CAPTIONS

Figure 1. Model initial analyses of the surface-based CIN (J kg^{-1}) valid 0000 UTC 25 April 2008 for the area centered on western Kansas. Models include the: (a) Local Analysis and Prediction System (LAPS); (b) Rapid Update Cycle (RUC); (c) North American Mesoscale (NAM); and (d) Global Forecasting System (GFS). Values of SBCIN $< -30 \text{ J kg}^{-1}$ are shaded, with the darkest shading representing SBCIN $< -250 \text{ J kg}^{-1}$.

Figure 2. Observed skew T -log p sounding (thick solid lines) for Rapid City, SD, valid 1800 UTC 25 July 2001. Half, whole, and flag wind barbs denote 2.5, 5, and 25 m s^{-1} , respectively. Temperature is given along the abscissa ($^{\circ}\text{C}$) and pressure is plotted along the ordinate (mb). The moist adiabat for the 1000-m mixed-layer parcel is highlighted by the bold dotted line. The small black shaded region represents CIN₁ and the larger grey shaded region represents CIN₂.

Figure 3. Elevation map (m) of the contiguous United States (CONUS), which encompasses the study area herein. Stars represent radiosonde locations used for the correlation analysis in Table 1, and the box denotes the “High Plains” region which was used for the cumulative frequency analysis in Fig. 7.

Figure 4. Observed skew T -log p soundings (thick solid lines) for Bismarck, ND, valid (a) 0000 31 July 2006 and (b) 0000 UTC 18 May 2007. Half, whole, and flag wind barbs denote 2.5, 5, and 25 m s^{-1} , respectively. Temperature is given along the abscissa ($^{\circ}\text{C}$) and pressure is plotted

along the ordinate (mb). The moist adiabat for the 1000-m mixed-layer parcel is highlighted by the bold dotted line.

Figure 5. Maximum T_{700} ($^{\circ}\text{C}$) associated with all convective severe storm reports from March to October, 1993–2006. The maximum T_{700} was determined from all reports in each of the roughly 80-km grid boxes, and then smoothing was applied by averaging 3×3 matrices and assigning the result to the center grid box (see section 2). White boxes denote areas with insufficient data. A color version of this figure is available at: <http://www.crh.noaa.gov/unr/?n=700mbTempsSvr>.

Figure 6. Empirical cumulative frequency distribution functions for T_{700} associated with all convective severe storm reports across the CONUS from 1993–2006 for each of the months from April to September.

Figure 7. Empirical cumulative frequency distribution function for T_{700} associated with all convective severe storm reports in the “High Plains” region outlined in Fig. 3 (28,282 reports, 9.5% of all CONUS reports). The bold dot signifies that 25.7% of the severe reports are associated with $T_{700} > 12^{\circ}\text{C}$.

Figure 8. Same as Fig. 5 except for monthly climatologies including (a) April, (b) May, (c) June, (d) July, (e) August, and (f) September.

Figure 9. Same as Fig. 5 except for partitions based on report type including (a) all tornadoes, (b) significant tornadoes, (c) all hail, (d) significant hail, (e) all wind, and (f) significant wind. Recall that only one report was required per grid box for the significant tornadoes (b), and thus these results should be interpreted with caution; if five reports per grid box would have been used then the area of (b) would only be 27% of its current size (see cross-hatched area; refer to section 2 for additional discussion).

Figure 10. Decile plots (i.e., dashes every 0%, 10%, ..., 100%) for report-type partitions versus T_{700} for (a) tornado rating, (b) hail diameter [1 in. = 2.54 cm], and (c) wind gust [1 kt = 0.5144 m s⁻¹]. Values in parentheses indicate the total number of CONUS-wide reports for that specific partition (e.g., there are 1018 tornadoes rated F2 from 1993–2006).

Figure 11. Same as Fig. 5 except for average 180-mb AGL MUCIN associated with all convective severe storm reports from March to October, 1993–2006.

Figure 12. Same as Fig. 6 except for 180-mb AGL MUCIN. In addition, the empirical cumulative frequency distribution is plotted for the “High Plains” region (see Fig. 3) for all months in the dataset (dotted line). This region includes 28,282 reports, or 9.5% of all CONUS reports.

TABLE CAPTIONS

Table 1. Correlation coefficients between T_{700} and various capping indices for seven sounding sites [Bismarck, ND (BIS); Nashville, TN (BNA); Boise, ID (BOI); Dodge City, KS (DDC); Green Bay, WI (GRB); Lake Charles, LA (LCH); and Midland, TX (MAF)]. Soundings from 1948–2008 that possessed $SBCAPE > 50 \text{ J kg}^{-1}$ were used in the calculations, except only the 1953–2008 period was available for GRB and MAF. A parcel with averaged values of θ and mixing ratio in the lowest 1000 m was used for the mixed-layer (ML) calculations; MU refers to the most-unstable parcel in the lowest 300 mb of the sounding; and SB refers to the surface-based parcel. The virtual temperature correction (Doswell and Rasmussen 1994) was used for all parcel calculations. Stations are ordered by decreasing elevation from left to right.

Table 2. Convective severe storm reports from 1993–2006 that were used in the present study (297,086 total). Significant severe weather reports in parentheses are as defined in Hales (1988): “Sig Torn” includes F2–F5 tornadoes; “Sig Hail” includes hail with diameter $\geq 5.1 \text{ cm}$ (2.0 in.); and “Sig Wind” includes wind gusts $\geq 33.4 \text{ m s}^{-1}$ (65 kt).

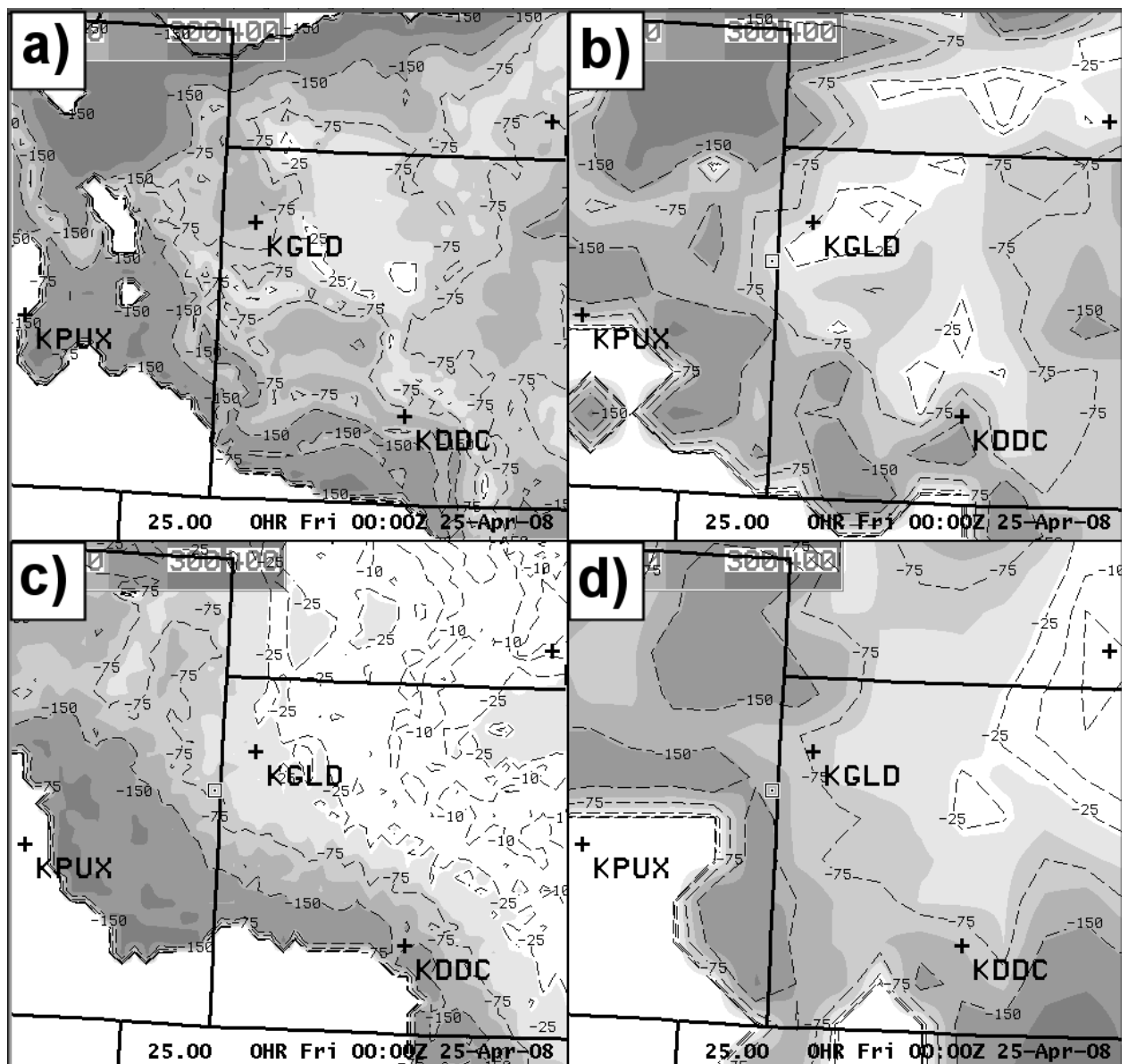


Figure 1. Model initial analyses of the surface-based CIN (J kg^{-1}) valid 0000 UTC 25 April 2008 for the area centered on western Kansas. Models include the: (a) Local Analysis and Prediction System (LAPS); (b) Rapid Update Cycle (RUC); (c) North American Mesoscale (NAM); and (d) Global Forecasting System (GFS). Values of SBCIN $< -30 \text{ J kg}^{-1}$ are shaded, with the darkest shading representing SBCIN $< -250 \text{ J kg}^{-1}$.

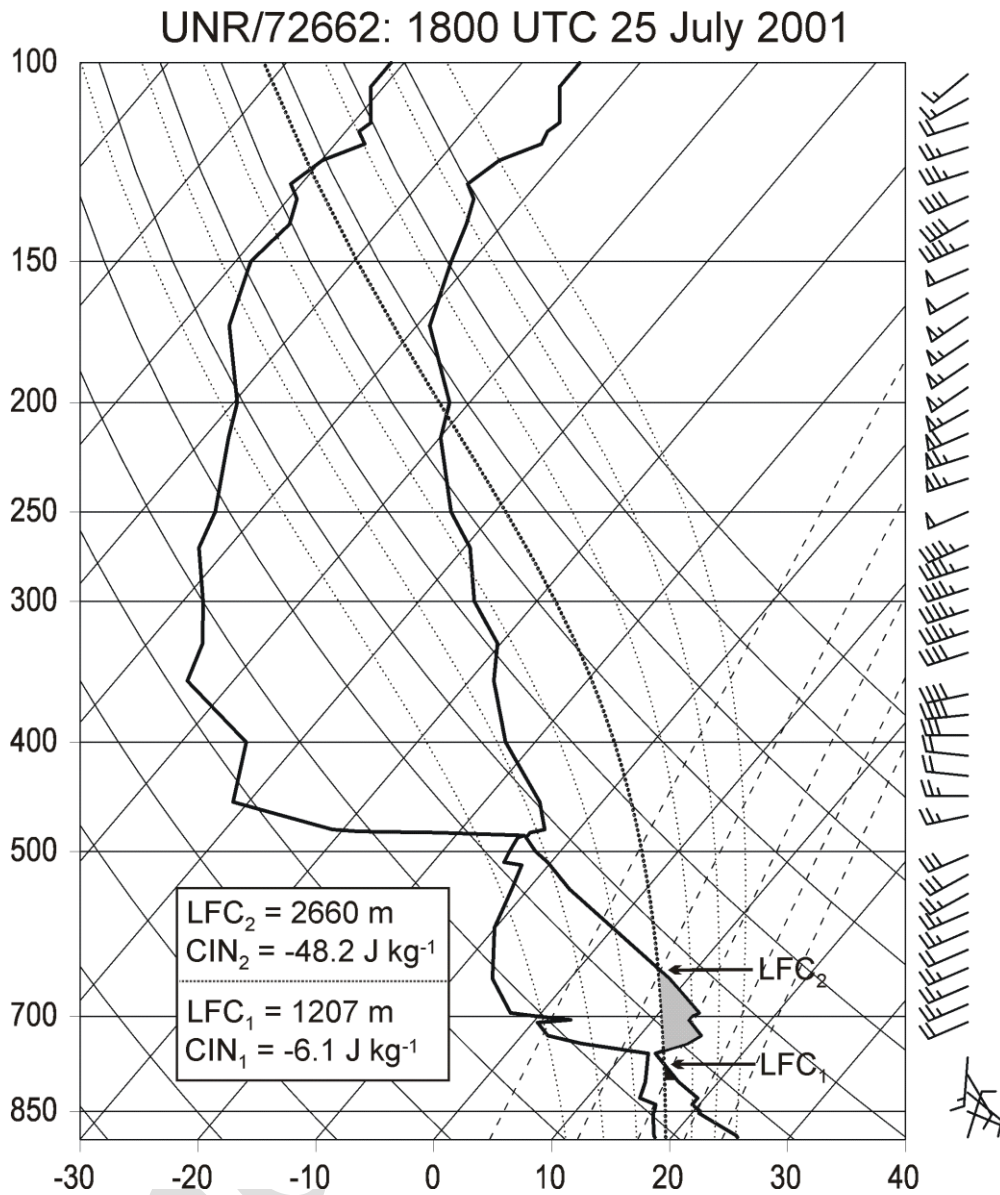


Figure 2. Observed skew T -log p sounding (thick solid lines) for Rapid City, SD, valid 1800 UTC 25 July 2001. Half, whole, and flag wind barbs denote 2.5, 5, and 25 m s⁻¹, respectively. Temperature is given along the abscissa (°C) and pressure is plotted along the ordinate (mb). The moist adiabat for the 1000-m mixed-layer parcel is highlighted by the bold dotted line. The small black shaded region represents CIN₁ and the larger grey shaded region represents CIN₂.

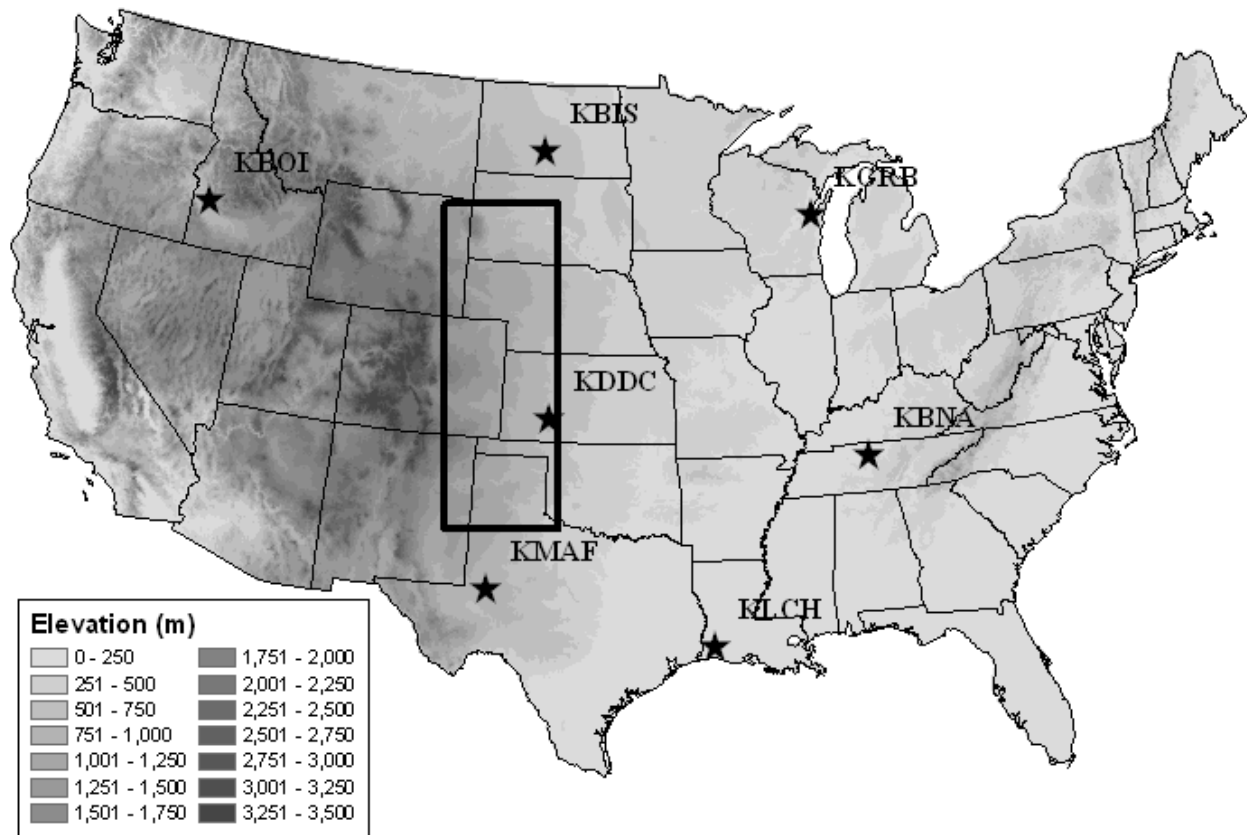


Figure 3. Elevation map (m) of the contiguous United States (CONUS), which encompasses the study area herein. Stars represent radiosonde locations used for the correlation analysis in Table 1, and the box denotes the “High Plains” region which was used for the cumulative frequency analysis in Fig. 7.

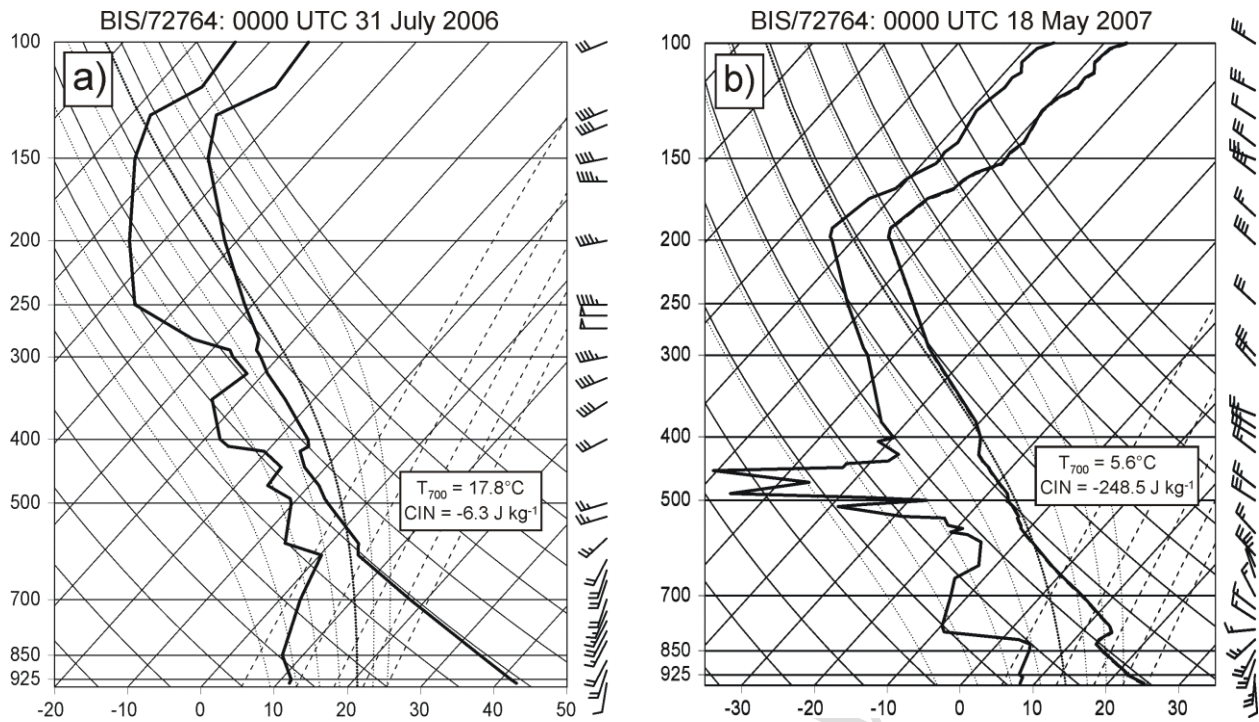


Figure 4. Observed skew T -log p soundings (thick solid lines) for Bismarck, ND, valid (a) 0000 31 July 2006 and (b) 0000 UTC 18 May 2007. Half, whole, and flag wind barbs denote 2.5, 5, and 25 m s^{-1} , respectively. Temperature is given along the abscissa ($^{\circ}\text{C}$) and pressure is plotted along the ordinate (mb). The moist adiabat for the 1000-m mixed-layer parcel is highlighted by the bold dotted line.

Smoothed Maximum 700-mb Temperature (All Severe Reports, Mar–Oct, 1993–2006)

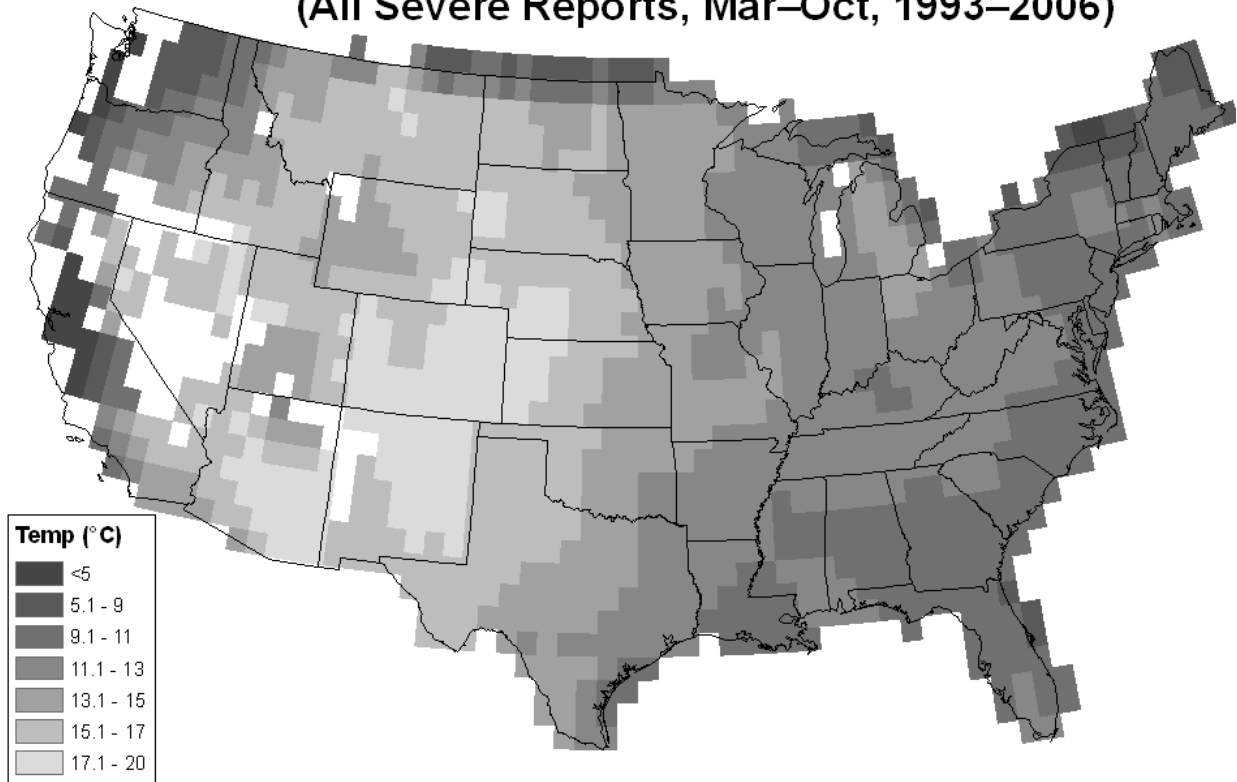


Figure 5. Maximum T_{700} ($^{\circ}\text{C}$) associated with all convective severe storm reports from March to October, 1993–2006. The maximum T_{700} was determined from all reports in each of the roughly 80-km grid boxes, and then smoothing was applied by averaging 3×3 matrices and assigning the result to the center grid box (see section 2). White boxes denote areas with insufficient data. A color version of this figure is available at: <http://www.crh.noaa.gov/unr/?n=700mbTempsSvr>.

CONUS Severe Weather Reports (1993–2006)

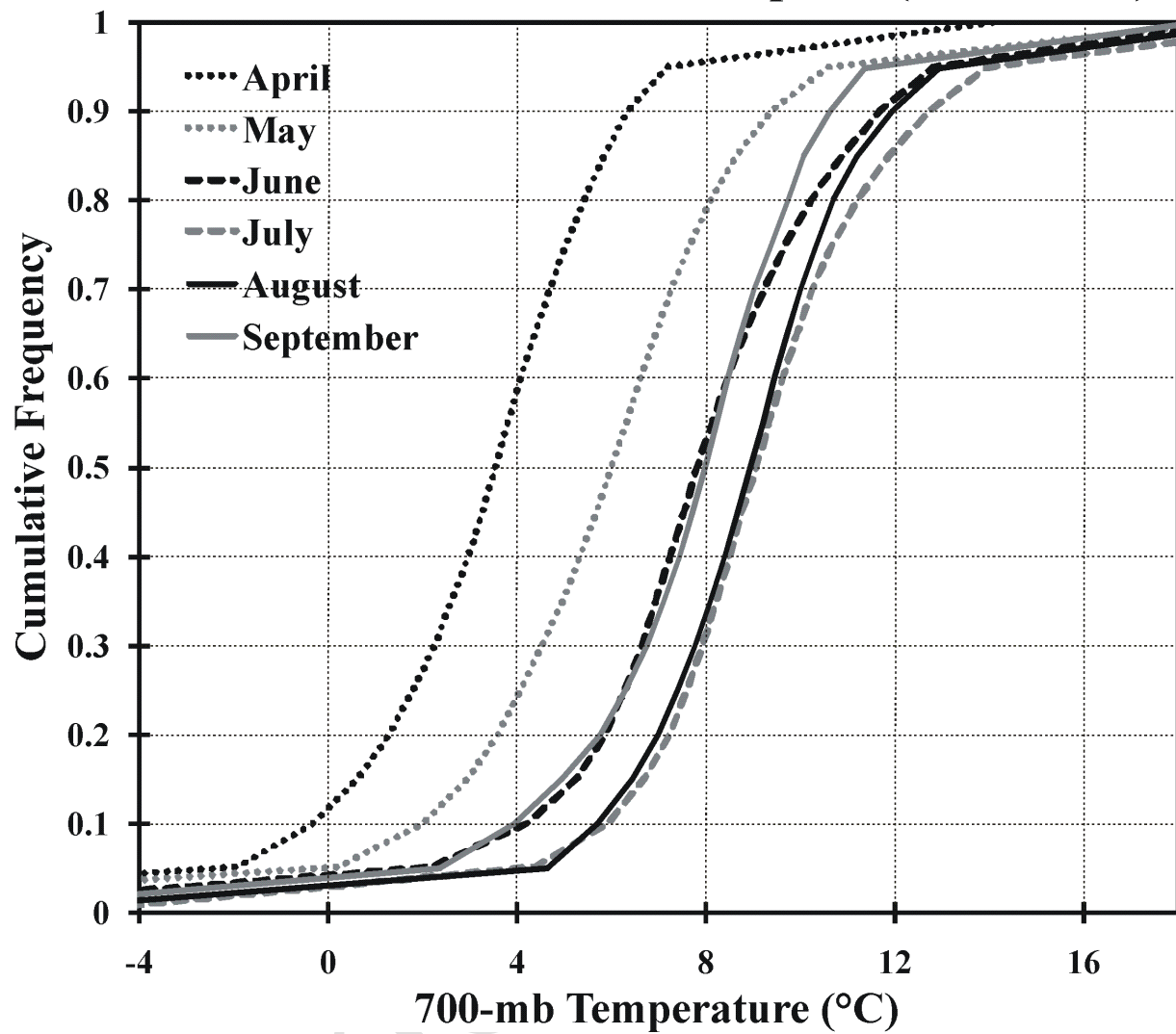


Figure 6. Empirical cumulative frequency distribution functions for T_{700} associated with all convective severe storm reports across the CONUS from 1993–2006 for each of the months from April to September.

“High Plains” Severe Weather Reports

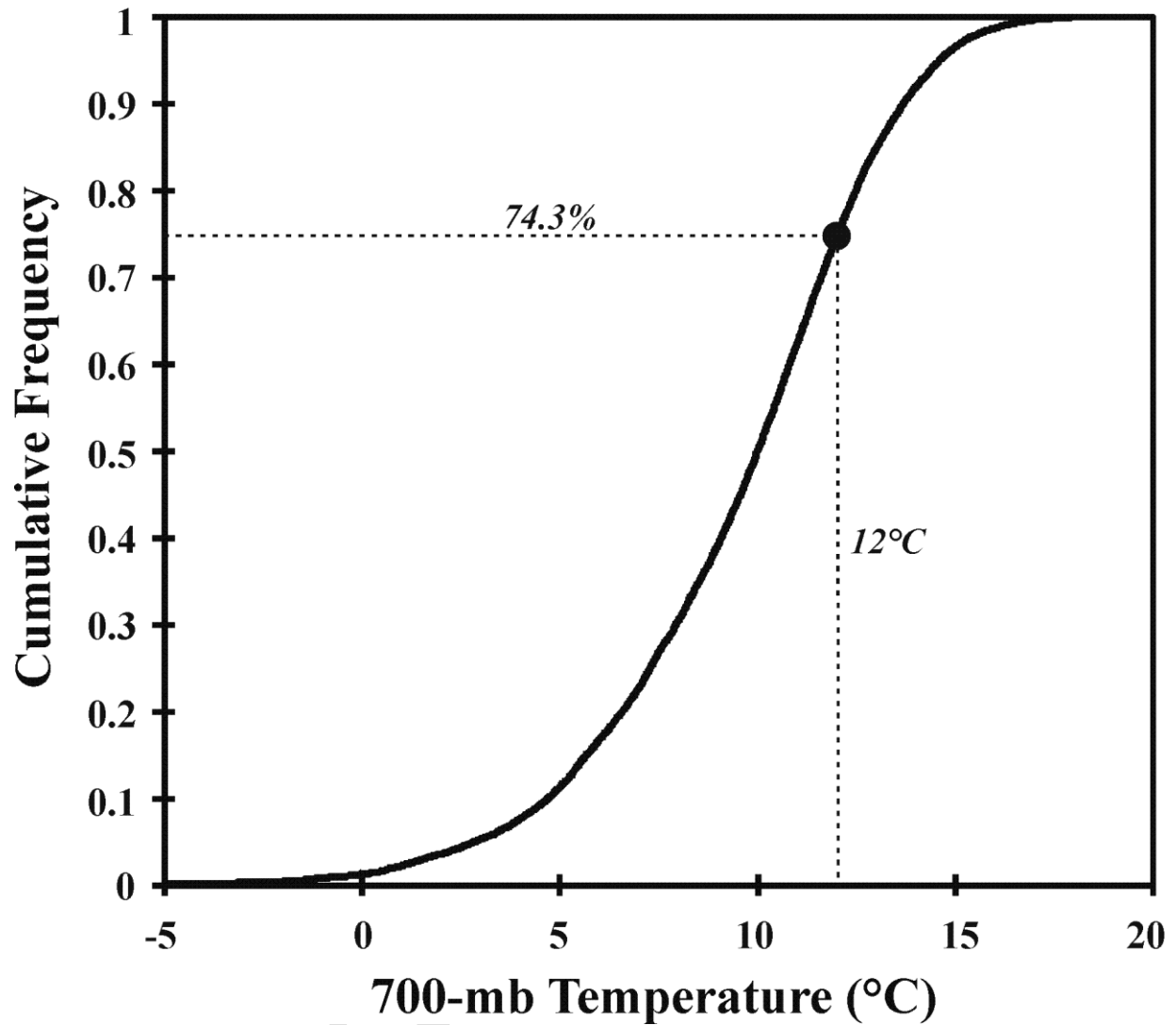


Figure 7. Empirical cumulative frequency distribution function for T_{700} associated with all convective severe storm reports in the “High Plains” region outlined in Fig. 3 (28,282 reports, 9.5% of all CONUS reports). The bold dot signifies that 25.7% of the severe reports are associated with $T_{700} > 12^{\circ}\text{C}$.

Smoothed Maximum 700-mb Temperature (All Severe Reports, Apr–Sep, 1993–2006)

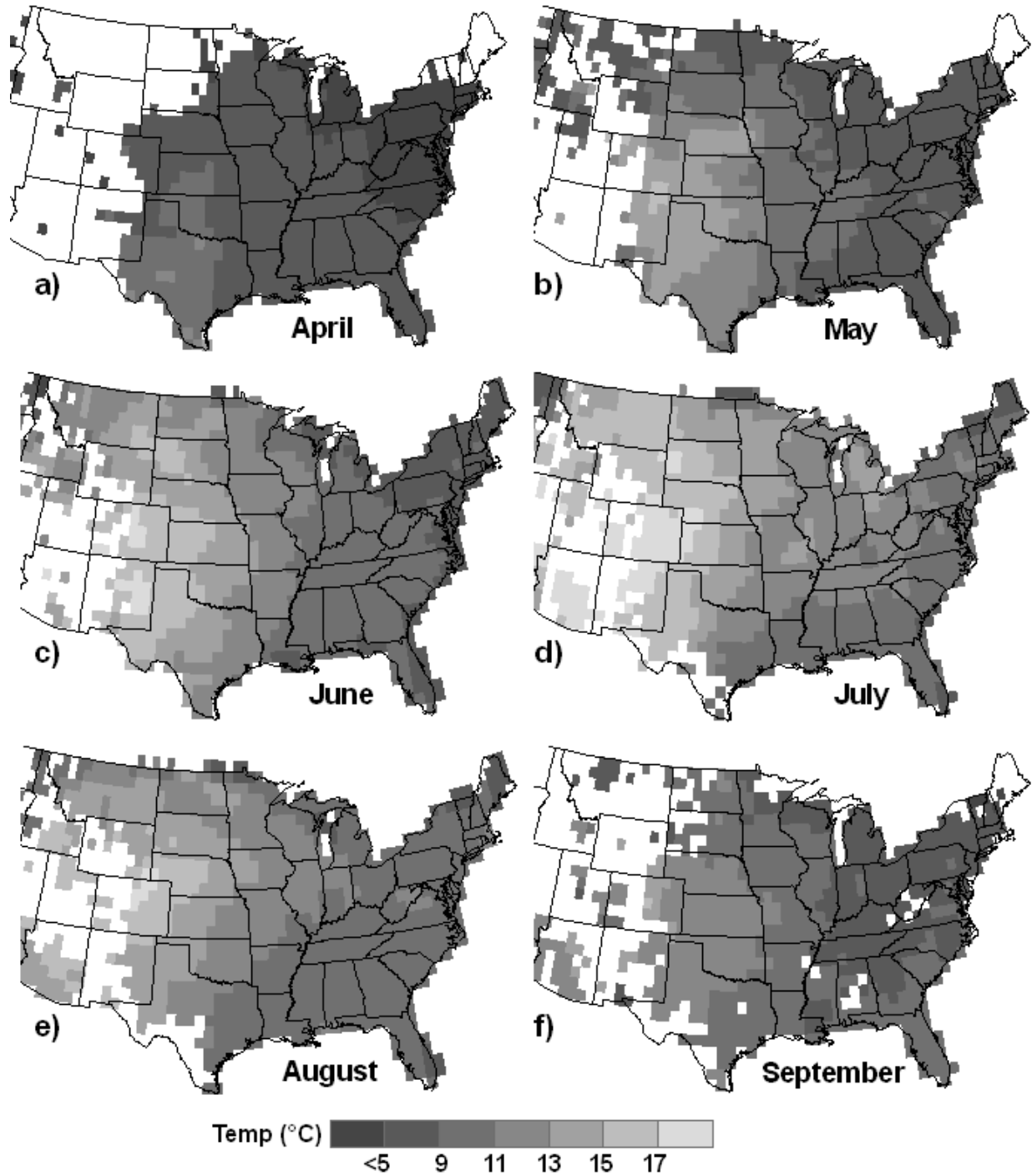


Figure 8. Same as Fig. 5 except for monthly climatologies including (a) April, (b) May, (c) June, (d) July, (e) August, and (f) September.

Smoothed Maximum 700-mb Temperature
(Torn, Hail, & Wind, Apr–Sep, 1993–2006)

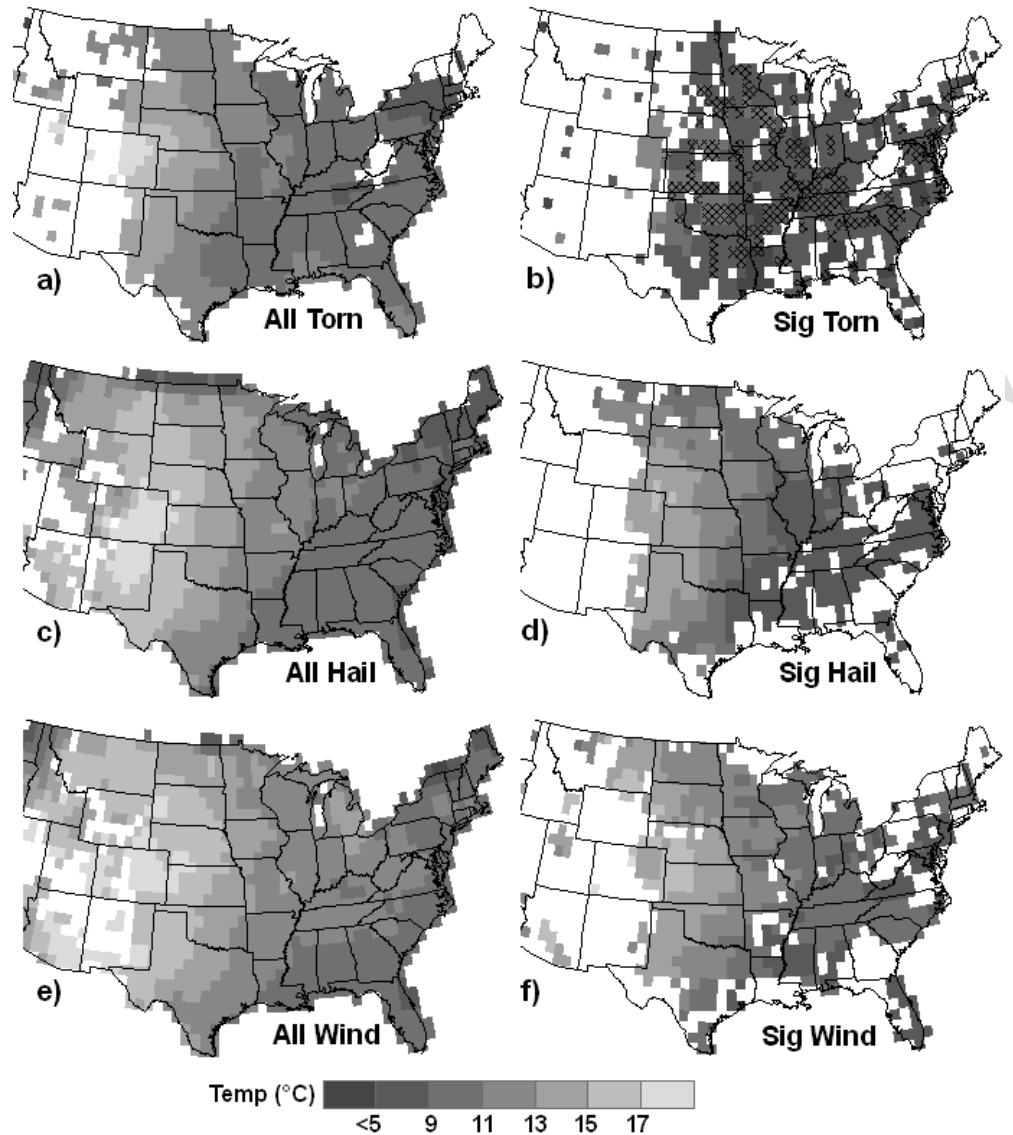


Figure 9. Same as Fig. 5 except for partitions based on report type including (a) all tornadoes, (b) significant tornadoes, (c) all hail, (d) significant hail, (e) all wind, and (f) significant wind. Recall that only one report was required per grid box for the significant tornadoes (b), and thus these results should be interpreted with caution; if five reports per grid box would have been used then the area of (b) would only be 27% of its current size (see cross-hatched area; refer to section 2 for additional discussion).

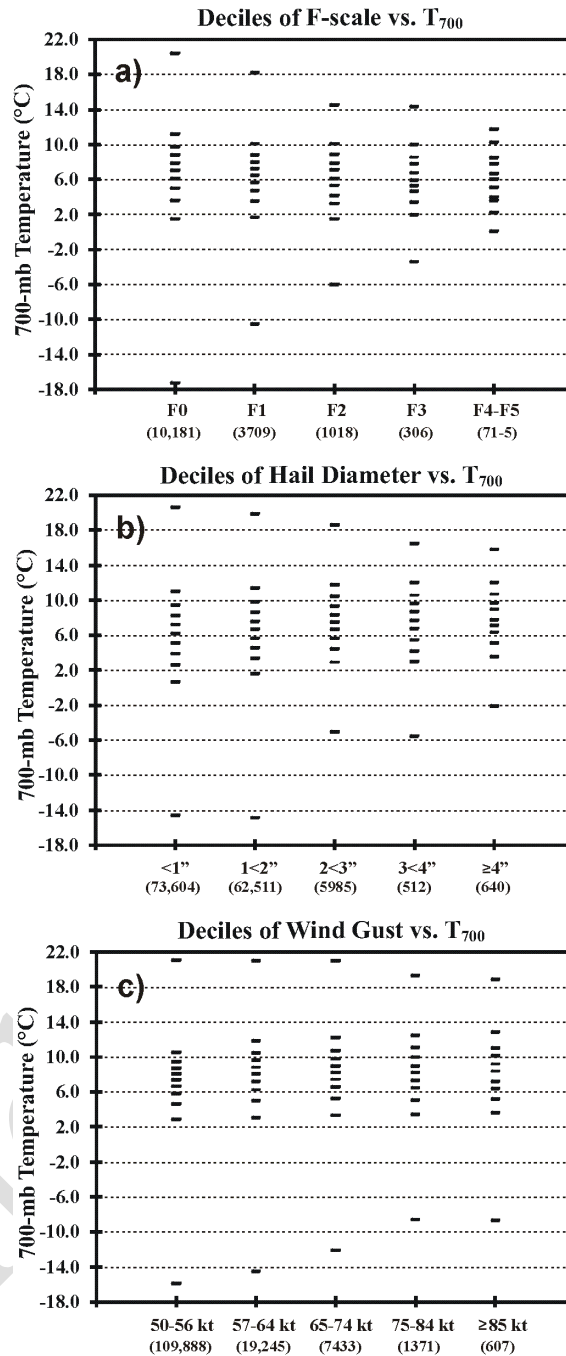


Figure 10. Decile plots (i.e., dashes every 0%, 10%, ..., 100%) for report-type partitions versus T_{700} for (a) tornado rating, (b) hail diameter [1 in. = 2.54 cm], and (c) wind gust [1 kt = 0.5144 m s^{-1}]. Values in parentheses indicate the total number of CONUS-wide reports for that specific partition (e.g., there are 1018 tornadoes rated F2 from 1993–2006).

Smoothed Average 180-mb AGL MUCIN
(All Severe Reports, Mar–Oct, 1993–2006)

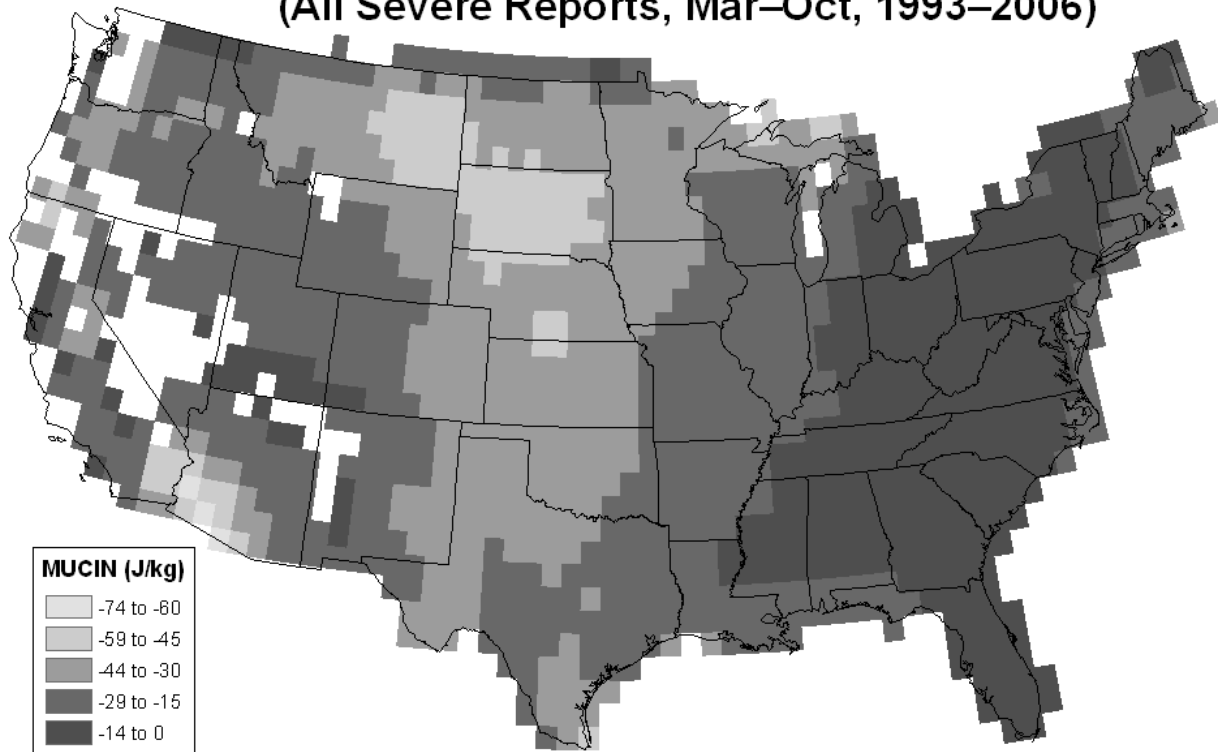


Figure 11. Same as Fig. 5 except for average 180-mb AGL MUCIN associated with all convective severe storm reports from March to October, 1993–2006.

CONUS Severe Weather Reports (1993–2006)

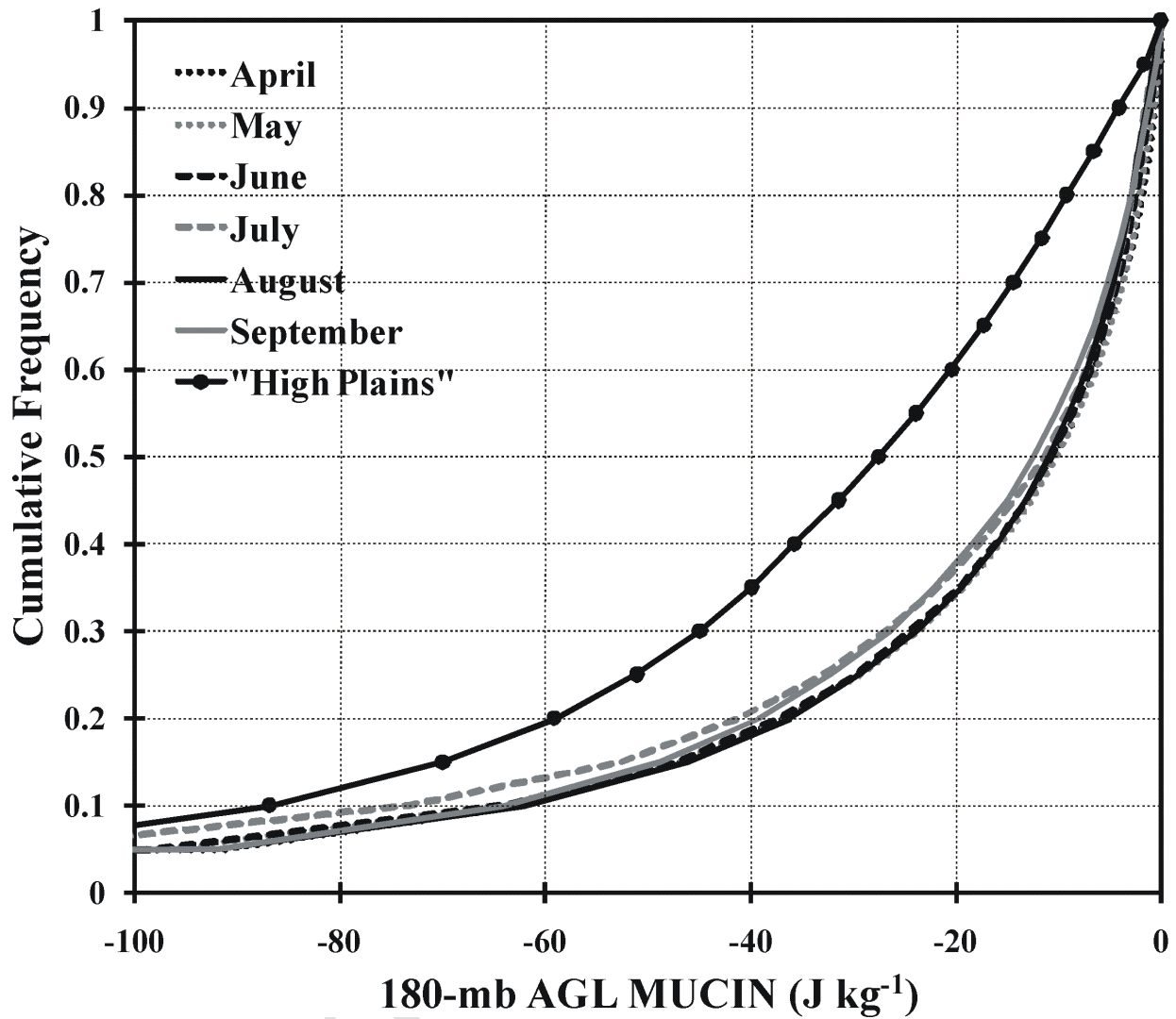


Figure 12. Same as Fig. 6 except for 180-mb AGL MUCIN. In addition, the empirical cumulative frequency distribution is plotted for the “High Plains” region (see Fig. 3) for all months in the dataset (dotted line). This region includes 28,282 reports, or 9.5% of all CONUS reports.

Correlations	MAF	BOI	DDC	BIS	GRB	BNA	LCH
T ₇₀₀ vs. MLCIN	-.31	-.51	-.36	-.50	-.36	-.19	-.14
T ₇₀₀ vs. MUCIN	-.27	-.44	-.31	-.41	-.26	-.13	-.09
T ₇₀₀ vs. SBCIN	-.28	-.43	-.33	-.45	-.34	-.20	-.08
T ₇₀₀ vs. LSI	.28	.17	.43	.47	.19	.08	.21

Table 1. Correlation coefficients between T₇₀₀ and various capping indices for seven sounding sites [Bismarck, ND (BIS); Nashville, TN (BNA); Boise, ID (BOI); Dodge City, KS (DDC); Green Bay, WI (GRB); Lake Charles, LA (LCH); and Midland, TX (MAF)]. Soundings from 1948–2008 that possessed SBCAPE >50 J kg⁻¹ were used in the calculations, except only the 1953–2008 period was available for GRB and MAF. A parcel with averaged values of θ and mixing ratio in the lowest 1000 m was used for the mixed-layer (ML) calculations; MU refers to the most-unstable parcel in the lowest 300 mb of the sounding; and SB refers to the surface-based parcel. The virtual temperature correction (Doswell and Rasmussen 1994) was used for all parcel calculations. Stations are ordered by decreasing elevation from left to right.

	Torn (Sig Torn)	Hail (Sig Hail)	Wind (Sig Wind)	Total (All Sig)
March	939 (165)	10,094 (362)	5499 (385)	16,532 (912)
April	2087 (276)	23,948 (1136)	11,384 (850)	37,419 (2262)
May	3786 (381)	36,625 (2070)	23,089 (1766)	63,500 (4217)
June	3242 (201)	30,532 (1587)	32,870 (2344)	66,644 (4132)
July	1986 (118)	19,408 (1031)	34,675 (2228)	56,069 (3377)
August	1223 (72)	12,992 (533)	20,760 (1278)	34,975 (1883)
September	1140 (102)	6086 (255)	6557 (360)	13,783 (717)
October	887 (85)	3567 (163)	3710 (200)	8164 (448)
Total	15,290 (1400)	143,252 (7137)	138,544 (9411)	297,086 (17,948)

Table 2. Convective severe storm reports from 1993–2006 that were used in the present study (297,086 total). Significant severe weather reports in parentheses are as defined in Hales (1988): “Sig Torn” includes F2–F5 tornadoes; “Sig Hail” includes hail with diameter ≥ 5.1 cm (2.0 in.); and “Sig Wind” includes wind gusts ≥ 33.4 m s⁻¹ (65 kt).